Ultrathin Films of Poly(ethylene oxides) on Oxidized Silicon. 1. Spectroscopic Characterization of Film Structure and Crystallization Kinetics

Holger Schönherr*,† and Curtis W. Frank*

NSF MRSEC Center on Polymer Interfaces and Macromolecular Assemblies (CPIMA) and Department of Chemical Engineering, Stanford University, Stanford, California 94305-5025

Received May 6, 2002; Revised Manuscript Received December 5, 2002

ABSTRACT: We have characterized the structure, molecular orientation, and crystallization kinetics of isothermally crystallized thin (film thickness d < 500 nm) and ultrathin films (d < 100 nm) of poly(ethylene oxides) on oxidized silicon substrates by a combination of microscopic and spectroscopic methods. In situ hot stage atomic force microscopy (AFM) reveals a preferred flat-on orientation of lamellar crystals in films thinner than ca. 300 nm. The mean orientation of the polymer molecules, as measured by transmission and grazing angle reflection FT-IR spectroscopy, fully agrees with the preferred orientation of the PEO helices parallel to the surface-normal direction, as inferred from the AFM data. In addition to a strong film thickness dependence of this preferred chain orientation, the FT-IR data indicate that the degree of crystallinity decreases steadily when the film thickness becomes smaller than ∼200 nm. The local environment of pyrene end-labels in derivatized PEO was characterized by steady-state fluorescence spectroscopy, and the excimer/monomer emission ratio was found to be very sensitive to both film thickness and crystallization temperature. The latter relationship could be described by an Arrhenius equation and yielded an excimer-forming-site energy of 17 ± 2 kJ/mol. Finally, the isothermal crystallization of PEO in ultrathin films was followed spectroscopically in situ. Both fluorescence and FT-IR spectroscopy indicated that the crystallization kinetics are progressively slowed down for decreasing film thickness, presumably due to the increased glass transition temperature of ultrathin PEO films on interactive substrates.

Introduction

Thin (<500 nm) and ultrathin films (<100 nm) of polymers[1,2] are used in numerous applications and processes, including alignment layers for liquid crystals in displays,[3] photoresists for photolithography,[2,4] boundary layer lubricants in data storage applications,[5] sensors,[6] and antireflection coatings.[7] Recently, layer-by-layer deposited polyelectrolyte thin films[8] have been utilized to fabricate versatile *functional* micro- and nanocapsules, which possess considerable potential for applications in many fields, including drug delivery.[9] The physical behavior of polymers in confinement, such as in ultrathin films,[2] block copolymers,[10−12] or nanocomposites,[13] may differ considerably from the behavior observed in the bulk. Depending on the thickness of ultrathin films, the glass transition temperature,[14−21] crystallization kinetics and degree of crystallinity,[22−24] phase behavior,[25,26] morphology,[27] permeability,[28] electrical properties,[29] moisture absorption,[30] or dewetting[31] may be altered. Recent experimental results by Kraus et al.[32] showed a significant distortion of the chain conformation by diffuse neutron scattering. These observations are supported by simulations that suggest disturbed single chain properties for polymer molecules near a wall in the melt.[33] Parallel to the surface, the conformation of the macromolecules in ultrathin films is retained according to small-angle neutron scattering data obtained by Jones et al.[34]

Much attention in the study of ultrathin polymer films has been focused on glassy polymers and in particular on the changes in glass transition temperature T_g with film thickness. Following the first report of a T_g depression observed by ellipsometry in ultrathin films of polystyrene on hydrogen-terminated silicon by Keddie et al.,[14] many different systems have been investigated.[14−21] The interpretation of the observed effects and the formulation of a unifying theory have been complicated by contradictory results on nominally the same polymer/substrate combinations.[35] Nevertheless, there seems to be evidence in the recent literature that T_g of substrate-supported ultrathin polymer films can either increase as a result of attractive interfacial interactions or decrease as a result of repulsive interfacial interactions.[36]

In addition to changes in glass transition temperatures, the confinement into ultrathin films has been reported to affect diffusion of the polymer molecules comprising the film[37−41] as well as diffusion of small, low-molar-mass tracer molecules.[35,42,43] These effects have sometimes been observed for film thicknesses up to several hundred nanometers, while the changes in T_g are of much shorter range (typically tens of nanometers).

The *crystallization* of polymers in confined geometries or constrained environments has also received considerable attention in recent years.[2,22−24,44−46] Since the T_g and molecular mobility of polymers in ultrathin films can be substantially altered due to interfacial interactions,[14−21,37−41] transport of polymer molecules to the growth front of a crystallizing polymer lamella is

† Present address: University of Twente, Faculty of Chemical Technology and MESA+ Research Institute, Department of Materials Science and Technology of Polymers, P.O. Box 217, 7500 AE Enschede, The Netherlands.

* Corresponding authors. H.S.: phone ++31 53 489 3170; Fax ++31 53 489 3823; e-mail h.schonherr@ct.utwente.nl. C.W.F.: phone 650 723-4573; Fax 650 723-9780; e-mail curt@chemeng.stanford.edu.

10.1021/ma020685i CCC: $25.00
Published on Web 01/31/2003

expected to be affected.[47] This may lead to changes in the crystallization kinetics[22−24] and potentially to changes in morphology if a competing, but kinetically unfavorable, process becomes dominating as a result of the reduced effective diffusion coefficient. In block copolymers the crystallization of poly(ethylene oxide) blocks was found to be affected by the confinement between glassy blocks of polystyrene,[11] while in nanocomposites the collectivity of macromolecular motions and the corresponding relaxation behavior can be altered due to isolation of polymer chains.[48]

For ultrathin films of poly(di-*n*-hexylsilanes) on glass and quartz substrates, our group has shown that the crystallization kinetics and the degree of crystallinity are strong functions of film thickness.[2,22,23] The growth rates were fitted to the Avrami equation,[49] and the Avrami exponent n was found to depend on both the film thickness d and crystallization temperature T_c.[2,22] In particular, the transition from 3-D bulk crystallization to 1-D growth at high T_c and low film thicknesses clearly showed that confinement into ultrathin films can substantially alter the crystallization behavior.

In addition, the orientation of the poly(di-*n*-hexylsilane) molecules depended on film thickness. Such an existence of an energetically preferred orientation can be expected to affect the crystallization process of the polymer. For example, the poly(di-*n*-hexylsilane) backbones are oriented preferentially in the plane of the film. Similar interfacial effects are also present for self-assembled thin film blends of poly(ethylene oxide) and poly(methyl methacrylate) on glass,[50] layers of high-density polyethylene on calcite and rubber,[45] nylon-6 on rubber,[51] or polyimide on silicon.[52] In our studies on ultrathin films of polypropylenes,[53,54] as well as poly(ethylene oxides) (PEO)[53] on oxidized silicon substrates, we have seen evidence for similar preferred orientations. While polypropylene crystallized with lamellae in edge-on orientation, i.e., with the polymer chain axis in the plane of the film, for essentially all film thicknesses, the PEO lamellae showed an interesting film thickness dependent morphology.

This paper is a first in a series in which we address the crystallization behavior of poly(ethylene oxide) in ultrathin films on oxidized silicon substrates.[53,55,56] PEO is a particularly well-suited model system for the investigation of crystallization of polymers, and a large body of literature on bulk crystallization is available.[57] PEO usually crystallizes in a monoclinic phase where the polymer chains adopt a $^7/_2$ helix.[58] Stretching of the polymer results in a planar zigzag conformation with a triclinic crystal structure.[59] In this first paper we report on the infrared and fluorescence spectroscopic characterization of the film structure and crystallization kinetics of spin-coated films of PEO and pyrene end-labeled PEO on oxidized silicon. A more detailed quantitative study of the crystallization kinetics by means of in situ hot stage AFM[60] and fitting of the growth rate data based on the Hoffman−Lauritzen theory[47,55b] will be presented in a companion paper.[55c]

Experimental Section

Materials and Sample Preparation. Poly(ethylene oxide) (PEO, M_w = 100 000 g/mol, Polysciences), pyrene end-labeled PEO (PEOpy, M_w (relative to PS): 49 340 g/mol (M_w/M_n = 2.06), 28 930 g/mol (M_w/M_n = 1.91), 10 800 g/mol (M_w/M_n = 1.03)),[61] and chloroform (Mallinckrodt) were used without further purification. The PEO materials are denoted PEO-100, PEOpy-49, PEOpy-29, and PEOpy-11, respectively. Thin films of PEO were prepared by spin-coating filtered (Millex-G PTFE filters, 0.20 μm, Millipore, Bedford, MA) solutions of PEO in chloroform with concentrations between 1.0 and 50.0 mg/mL onto argon-plasma-cleaned (March Plasmod, March Instruments, Concord, CA) single-side or double-side polished silicon wafers using a model CB15 spin-coater (Headway Research, Garland, TX) at 3300 rpm for 1 min. The static contact angles measured with water on the bare substrates were <5°. After the film preparation, the films were dried for at least 24 h in a vacuum. Thicknesses were determined by ellipsometry (Gaertner L 166C, Skokie, IL; wavelength 632.8 nm, 70° angle of incidence, polarizer set to 45°) assuming the refractive index n_f to be 1.454 and additionally by profilometry using AFM. A well-defined thermal history for samples investigated systematically by FT-IR and fluorescence spectroscopy was ensured by melting samples at 75 °C on a custom-built hot stage (based on a model PC-600 hotstage, Corning, Acton, MA) equipped with a temperature controller (CSS-8094 Omega, Stamford, CT) in an argon atmosphere. After melting, the samples were crystallized isothermally to completion under argon and quenched to room temperature. To ensure a consistent thermal history, all samples with a given thermal history were prepared simultaneously.

FT-IR Spectroscopy (FT-IR). The FT-IR data were obtained on a BIO-RAD FTS-60A FT-IR spectrometer operated in transmission mode (DTGS detector) and a Perkin-Elmer Spectrum 2000 FT-IR operated in grazing incidence reflection (GIR) mode (liquid nitrogen cooled MCT detector) using a Graseby Specac GIR accessory (angle of 75° with respect to surface-normal direction, p-polarization). The FT-IR spectrometers were purged continuously with dried air. A total of 512−1024 scans were collected with a resolution of 2 or 4 cm^{-1} and ratioed against the previously collected background spectrum. The bulk spectra were recorded in transmission mode using a thick film (d > 20 μm) of PEO supported on a silicon wafer. The kinetic data were acquired using a home-built heating stage (connected to a Cole Parmer EW-02155-56 temperature controller, Cole Parmer, Vernon Hills, IL) and the Perkin-Elmer "Timebase" software package. Thirty-two or 64 scans were averaged per spectrum. The fastest sampling time was 36 s per data point.

Steady-State Fluorescence Spectroscopy. Steady-state fluorescence emission spectra were collected with a Edinburgh Instruments CD900 spectrometer and a 500 W xenon lamp in front-face illumination geometry.[62] To avoid photooxidation of the pyrene moieties, the sample chamber was purged with high-purity argon. The excitation wavelength λ_{exc} was set to 343 nm, emission spectra were collected between 360 and 650 nm using slit widths between 0.5 and 1.5 mm, and sampling times were 0.5−1.0 s. Spectra were acquired at three different locations of each sample. For kinetic experiments, the fluorescence emission intensity of the excimer was measured at 480 nm (λ_{exc} = 343 nm) using slit widths of up to 3.5 mm. For the in situ measurements of the crystallization kinetics, a similar heating stage as for the FT-IR experiments was used. All the spectra shown here were baseline corrected.

Atomic Force Microscopy (AFM). The AFM data shown here were acquired with a NanoScope III multimode AFM operated in tapping mode (Digital Instruments (DI), Santa Barbara, CA) using microfabricated silicon tips/cantilevers (Nanosensors, Wetzlar, Germany). AFM images were captured in ambient atmosphere (ca. 30% relative humidity, 24 °C temperature[63]) or at elevated temperatures using a custom-built hot stage (vide infra) in ambient or dry argon atmosphere. Height, phase, and amplitude images were collected simultaneously using a set point ratio of ∼0.9 for measurements at room temperature and a set point ratio of 0.6−0.7 for hot stage work. All images were subjected to a first-order plane-fitting procedure to compensate for sample tilt. The home-built AFM hot stage is based on a dc powered Peltier element attached to a machined Teflon spacer (for details see ref 55b). On top of the Peltier element a small thermocouple was attached to monitor the surface temperature, which was additionally calibrated against the melting points of a series of *n*-alkanoic acids.[55b] For the determination of the film thicknesses by

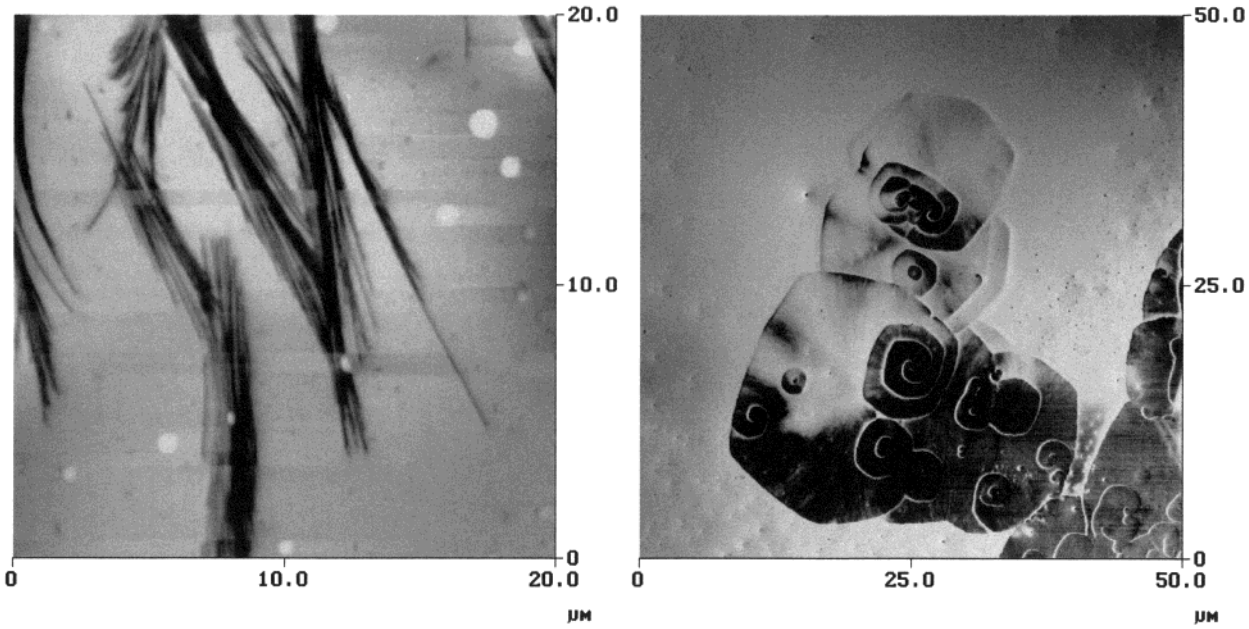

Figure 1. TM-AFM phase images of PEOpy-49 films with various thicknesses on oxidized silicon (images were acquired in situ at ca. 57 °C): thickness of ca. 2.5 μm (left) and 110 nm (right). In both films the featureless areas correspond to the polymer melt, which has not yet crystallized.

profilometry, the film was removed by scratching the samples using sharp tweezers (width of scratch between 15 and 30 μm). AFM height images measured in tapping mode (TM) as well as contact mode (using V-shaped Si_3N_4 cantilevers (DI) with a nominal spring constant of ~0.3 N/m) were subjected to a first-order plane fit followed by a cross-section analysis. An accurate calibration of the AFM scanner in the *z*-direction was ensured by using a set of three vertical calibration standards (TGZ 01−03) with step heights of 25, 104, and 515 nm, respectively (Silicon-MDT, Moscow, Russia, purchased from K-TEK International, Portland, OR).

Results

Atomic Force Microscopy. The morphology of spin-coated and subsequently isothermally recrystallized PEO films on oxidized silicon surfaces depends critically on film thickness (Figure 1). For PEO films with thicknesses of ca. 1 μm and thicker, crystallization occurs preferentially in the form of edge-on lamellar crystals (Figure 1, left),[64] whereas thinner films show predominantly flat-on lamellae (Figure 1, right). Note the numerous well-developed growth spirals in the right image, which are due to screw dislocations.[65] Films thinner than 300 nm crystallize *exclusively* in the form of flat-on lamellae that possess various inclination angles with respect to the film surface. With decreasing film thickness, the angles decrease until eventually at 10−20 nm thickness, depending on the crystallization temperature, the lamellae become thicker than the original average film thickness. Lamellae for these very thin films lie exactly in the plane of the film. Films thinner than 15 nm tend to break up and crystallize with a dendritic habit (see Figure S1 of Supporting Information). We have seen no qualitative differences among the different PEO and PEOpy materials studied. The flat-on orientation in films thinner than 300 nm seems to be energetically favorable since intentionally nucleated edge-on lamellar crystals rotate into the plane of the film and continue to grow as flat-on lamellae. This process can be followed in real-time by hot stage AFM.[55b,c] The final morphology of such a film is shown in Figure 2. Edge-on lamellae oriented in perpendicular direction occur in the central region, while the outer regions consist of flat-on lamellae. These observations were made consistently for crystallization temperatures between ca. 47 and 61 °C.

The AFM observations imply a preferred orientation of the polymer chain axis along the surface-normal direction for lamellae grown at the surface of films thinner than 300 nm. With decreasing film thicknesses, the orientational preference becomes qualitatively more pronounced because the tilt angles of the lamellae decrease. While it is in principle possible to determine the orientation of the PEO lamellae quantitatively by image analysis, this information would only characterize the polymer−air interface of the film. The measured lamellar thicknesses of these films are between ca. 10 and 20 nm, depending on the crystallization temperature.[55b,c] Thus, spectroscopic methods are needed in order to characterize the mean orientation of all the molecules in the films completely (vide infra).

FT-IR Spectroscopy. The preferred orientation of lamellar crystals in thin and ultrathin films of PEO on oxidized silicon substrates was interrogated by infrared spectroscopy. By comparing transmission mode and (p-polarized) GIR FT-IR spectra, the dipole transmission moments in the plane of the film and perpendicular to the plane of the film, respectively, can be analyzed separately. The complete band assignment for the observed vibrational transitions can be made on the basis of the classic analysis by Yoshihara et al.[66] and the thin film work by Hoffman and Rabolt.[50] The conformation of PEO in the solid state can be described as a $^7/_2$ helix. Analysis of the symmetry shows that vibrational transitions are polarized either parallel or perpendicular to the helical axis; thus, the vibrational spectra yield rich orientational information.[66]

Typical bulk transmission, thin film transmission, and GIR FT-IR spectra for PEOpy-49 crystallized isothermally at 47 °C are compared in Figure 3. The transmission FT-IR spectrum of the bulk sample is indistinguishable from the bulk spectra reported in the literature and, hence, represents an isotropic sample.

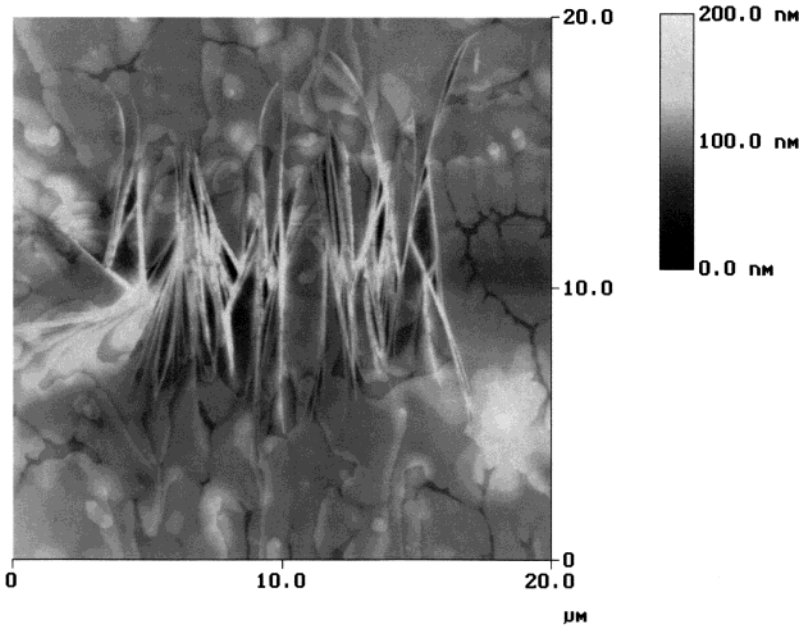

Figure 2. TM-AFM height image of a 128 nm thick PEO-100 film on oxidized silicon acquired at room temperature after completion of crystallization at ca. 57 °C. The lamellae were nucleated by dragging the tip through the melt along a horizontal line with a length of 15 μm.

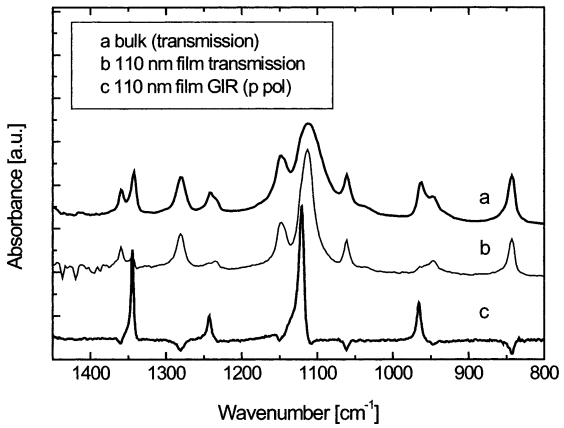

Figure 3. Transmission FT-IR spectrum of bulk sample compared with transmission and GIR (p polarized) FT-IR spectra of PEOpy-49 thin films on oxidized silicon (all samples were crystallized isothermally at 47 °C).

Important modes are the C−O stretching vibration at ca. 1107−1120 cm^{-1}, the CH_2 twisting vibrations at 1278 and 1240 cm^{-1}, the CH_2 wagging motion at 1360 and 1344 cm^{-1}, the CH_2 rocking vibration at 966 and 947 cm^{-1}, and the combination bands at 1060 cm^{-1} (ν(CO) + r(CH_2) + ν(CC)) and at 843 cm^{-1} (r(CH_2) + ν(COC)). Many bands in the GIR FT-IR spectra have negative absorbance, which is well-known for GIR FT-IR spectra on nonmetallic surfaces. However, without quantitative modeling of the IR spectra, a quantitative analysis of the absorbances and calculation of molecular orientation is not possible.[67] The complete band assignment and the polarization of the vibrations with respect to the helix axis are summarized in Table 1.

The wagging (1360, 1344 cm^{-1}) and rocking (966, 947 cm^{-1}) modes as well as the combination band at 843 cm^{-1} are very sensitive to conformational order, while the (CH_2) twist (1281, 1243 cm^{-1}) and the bands at ca. 1120 and 1107 cm^{-1} are not sensitive.[68]

A comparison of the spectral bands of the thin film spectra with the isotropic bulk spectrum shown in Figure 3 indicates that for the thin film sample the vibrations that are polarized perpendicular to the helix axis of PEO possess strong absorbance in the transmission spectra but weak absorbance in the GIR spectra. Likewise, the bands with parallel polarization with respect to the helix axis are weak in the thin film transmission spectra and strong in the GIR spectra.[69] On the basis of the mutually perpendicular orientation of the electric field vector for transmission vs grazing angle (with p-polarized light) modes, we conclude that the PEO helices are oriented preferentially along the surface-normal direction in thin films. This result is fully consistent with the orientation of lamellar crystals at the surface of the PEO films as imaged by tapping mode AFM (vide supra); i.e., the orientation of the PEO helices as determined from the lamellar crystals at the film surface and the molecular orientation in the "bulk" of the film are qualitatively very similar.

Figure 4 shows typical GIR FT-IR spectra of PEOpy-49 films of different thicknesses crystallized isothermally at 40 °C. Among others, the methylene wagging and twisting bands with perpendicular polarization with respect to the helix axis (see Table 1) show reduced absorbance relative to parallel polarized bands as film thickness decreases. This observation indicates that the preferential orientation depends on film thickness.

The effect of film thickness on polymer chain orientation was assessed more quantitatively by analyzing the absorbance of the bands at ca. 1240 and 1278 cm^{-1} in GIR FT-IR spectra of PEOpy-49. These transitions are polarized parallel to the helix axis and perpendicular to the helix axis, respectively, and are insensitive to the conformational order.[68] The ratio of these absorbances provides a measure for the orientation, as shown in Figure 5. For isothermal crystallization temperatures of 40, 44, and 47 °C, the polymer chains are preferentially oriented along the surface-normal direction. The preference depends strongly on film thickness, but it does not seem to depend significantly on the crystallization temperature in this range.[70]

Table 1. Band Assignment and Polarization of Relevant IR Transitions Observed in Crystallized PEO Films

band assignment (refs 50, 66)[a]	polarization (with respect to helix axis)[b]	wavenumber [cm^{-1}] (ref 66)	wavenumber transmission mode [cm^{-1}] (this study)	wavenumber GIR (p-pol) [cm^{-1}] (this study)
w(CH_2)	⊥	1358	1359	1360
w(CH_2)	||	1342	1343	1344
t(CH_2)	⊥	1278	1279	1281
t(CH_2)	||	1240	1241	1243
ν(CO)	⊥	1147	1146	1150
ν(CO)	⊥	1116	1115	1120
ν(CO)	||	1103	*c*	1107
ν(CO) + r(CH_2) +ν(CC)	⊥	1060	1062	1062
r(CH_2) + ν(CH_2)	||	958	961	966
r(CH_2) + ν(CC)	⊥	947	946	947
r(CH_2) + ν(CO)	⊥	844	843	843

[a] ν = stretch, r = rock, w = wag, t = twist. [b] ⊥ and || denote perpendicular polarization and parallel polarization, respectively, with respect to the helix axis of PEO. [c] Not resolved.

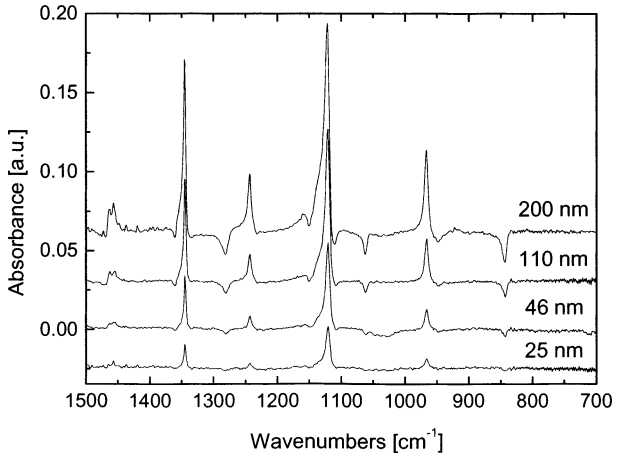

Figure 4. GIR FT-IR spectra (p-polarized) of PEOpy-49 films on oxidized silicon with different thicknesses crystallized isothermally at 40 °C.

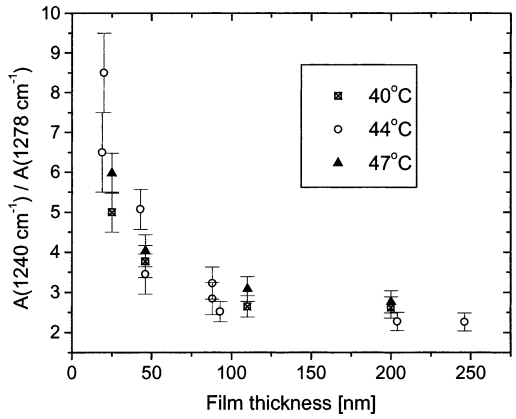

Figure 5. Ratio of integrated absorbance at ca. 1240 cm^{-1} to that at ca. 1278 cm^{-1} in GIR FT-IR spectra as a function of film thickness for PEOpy-49 films on oxidized silicon crystallized isothermally at different temperatures.

In addition, we found that the degree of crystallinity decreases with decreasing film thickness. As mentioned above, the band at ca. 843 cm^{-1}, for instance, is sensitive to the conformational order, while the strong band at ca. 1120 cm^{-1} is insensitive.[68] Both bands correspond to transitions having perpendicular polarization with respect to the helix axis. Thus, by normalizing the FT-IR spectra to the absorbance at ca. 1120 cm^{-1}, the dependence of conformational order on film thickness can be assessed. Since this cannot be easily translated into percent crystallinity, the result is only qualitative. From the plot of the relative absorbance of the band at

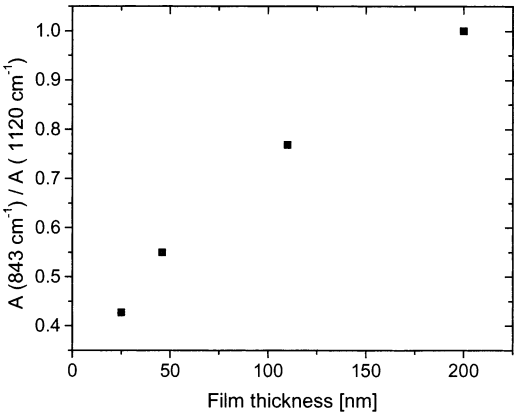

Figure 6. Absorbance at ca. 843 cm^{-1} (normalized to the absorbance at ca. 1120 cm^{-1}) as a function of film thickness estimated from GIR FT-IR spectra of different films of PEOpy-49 on oxidized silicon crystallized isothermally at 40 °C.

843 cm^{-1} (Figure 6) it is evident, however, that the conformational order decreases with decreasing film thickness. A comparable decrease in degree of crystallinity has been reported for ultrathin films of poly(di-*n*-hexylsilane)[2,22,23] and for the confined crystallization of PEO in organic networks.[71]

Steady-State Fluorescence Spectroscopy. The film structure of the pyrene end-labeled ultrathin films can be characterized and further compared to thicker films using steady-state fluorescence spectroscopy. The ratio of excimer to monomer fluorescence of the pyrene labels yields interesting insights into the clustering of the end groups.[72,73] The fluorescence data discussed in this paper will exclusively deal with films made of PEOpy-49.[74]

In Figure 7 we have plotted the normalized steady-state fluorescence emission spectra of a 190 nm thin film of PEOpy-49 that has been crystallized isothermally at different temperatures. The spectra, which were acquired at room temperature, have been normalized to the most intense monomeric emission band located at 378 nm. The broad emission with a maximum at ca. 480 nm corresponds to the excimer emission. On the basis of the data shown in Figure 7, it is obvious that the excimer-to-monomer emission intensity ratio is sensitive to the differences in film structure owing to different crystallization temperatures. In addition, the excimer-to-monomer ratio also decreases with decreasing film thickness (Figure S3 of Supporting Information). This decrease is attributed to a dilution of the pyrene moieties in the increased fraction of amorphous phase present in the thinner films.

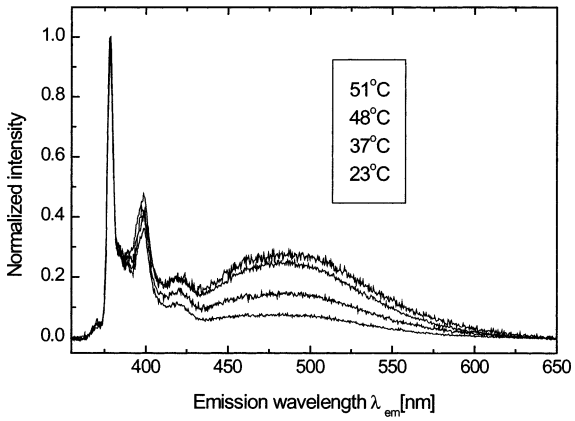

Figure 7. Normalized steady-state fluorescence emission spectra of 190 nm thick film of PEOpy-49 on oxidized silicon recorded at room temperature after isothermal crystallization at the specified temperature. The spectra have been normalized to the band at 378 nm, and the crystallization temperatures are indicated in the order of the spectra shown.

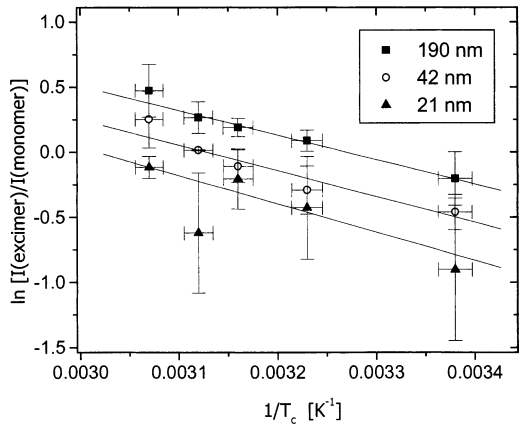

Figure 8. Linearized Arrhenius plots of excimer/monomer ratios observed by steady-state fluorescence spectroscopy for thin and ultrathin films of PEOpy-49 on oxidized silicon.

The temperature dependence can be described by an Arrhenius equation similar to the effect of casting temperature on excimer−monomer ratios observed by Frank for solvent-cast films of poly(4-vinylbiphenyl).[75] Analogously, we may postulate that each crystallization temperature corresponds to particular populations of the different environments of the chromophore in the semicrystalline PEO matrix. An activation energy is associated with the frozen populations of pyrene in different amorphous and crystalline environments. In this sense, the activation energy obtained from the Arrhenius plot shown in Figure 8 may be understood as an excimer-forming-site (EFS) energy. For PEOpy-49 we find a thickness-independent activation energy of 17 ± 2 kJ/mol. This value is of the same order of magnitude as the EFS energies of 8 and 15 kJ/mol observed for solution-cast films of poly(4-vinylbiphenyl) and poly(2-vinylnaphthalene),[75] respectively.

In Situ Crystallization Kinetics from FT-IR and Fluorescence Spectroscopy. The spectroscopic investigation of the crystallization process by means of FT-IR and fluorescence spectroscopy yields direct access to the mean crystallization kinetics in ultrathin films. In addition, the melting transitions can be studied. Using FT-IR spectroscopy, we followed conformationally sensitive vibrational bands (e.g., the (CH_2) wagging vibration at 1344 cm^{-1}) in real time, while in the steady-state fluorescence measurements the excimer emission intensity was measured in situ. Both methods show evidence for a substantially reduced growth rate in films thinner than ∼100 nm.

Figure 9 presents the changes in the FT-IR spectra during crystallization of a 204 nm film at 45 °C. The increase in absorbance of the three dominant modes in the spectral region shown, namely the (CH_2) wagging band at ca. 1344 cm^{-1}, the (CH_2) twist at 1243 cm^{-1}, and the C−O stretching vibration at ca. 1107−1120 cm^{-1}, is evident. In addition, the broad band at ca. 1150 cm^{-1}, which is typical of PEO in the melt, decreases rapidly in absorbance. The (CH_2) wagging band is particularly useful for study of the crystallization kinetics because the band is strong enough to yield sufficiently accurate data for very thin films and because there is no need for spectral deconvolution. The absorbance for the melt at ca. 1344 cm^{-1} is negligible; thus, this band can be exclusively attributed to the crystallized fraction of PEO.[68]

Typical changes in the IR absorbance at 1344 cm^{-1} were thus used to follow the crystallization of PEO films with different thicknesses, as shown in Figure 10. The data have been shifted to correct for different induction periods.

The different film thicknesses of the samples studied are responsible for the differences in magnitude of absorbance for the FT-IR data. Nevertheless, even without normalizing the data to maximum conversion of the process, the differences in kinetics are already evident. After an induction period, the absorbance increases before it levels off asymptotically. With decreasing film thickness, the crystallization takes longer to go to completion.

The fluorescence spectra also reveal the first order phase transition (Figure S4 of Supporting Information). It is also evident from the slopes of the normalized fluorescence intensity profiles shown in Figure 11 that the crystallization rate is slower in thinner films compared to thicker films. During crystallization, the fluorescence emission intensity for films thicker than ca. 50 nm decreased while for thinner films the intensity increased. This observation may suggest that the probability of excimer formation in the melt is a function of film thickness. However, for the measurement of crystallization kinetics only differential changes are important. Hence, the data shown in Figure 11 have been normalized correspondingly.

In Figure 12a we plot the half-crystallization time $\tau_{1/2}$ for various FT-IR experiments, which may serve as a crude measure for the crystallization rate. The $\tau_{1/2}$ for various samples as measured by fluorescence spectroscopy are shown in Figure 12b. The half-crystallization times depend on the crystallization temperature, which agrees with the usual behavior of polymers at low undercoolings. In addition to this expected dependence, $\tau_{1/2}$ varies significantly with the film thickness for all crystallization temperatures studied. The effect of confinement in thin and ultrathin films is pronounced for thicknesses below ca. 100 nm at sufficiently high crystallization temperatures. It is striking that the $\tau_{1/2}$ determined by FT-IR are much longer than the $\tau_{1/2}$ estimated from the fluorescence spectra.

Discussion

From the combined FT-IR and fluorescence spectroscopic data, it is evident that the confinement of PEO into thin and ultrathin films affects the film morphology,

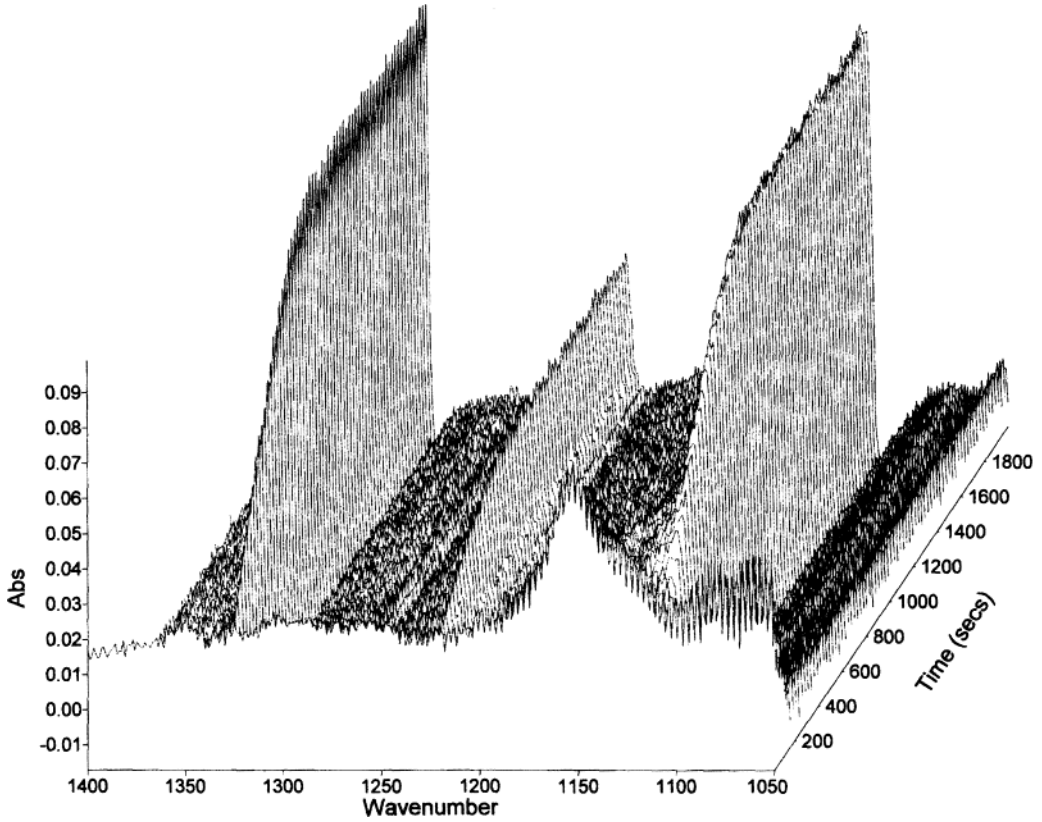

Figure 9. GIR FT-IR spectra (p-polarized) recorded at 45 °C in situ during crystallization of a 204 nm film of PEOpy-49 on oxidized silicon.

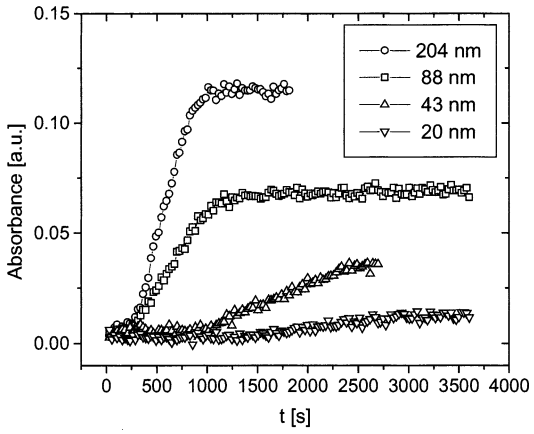

Figure 10. Integrated absorbance at 1344 cm^{-1} calculated from GIR FT-IR spectra (p-polarized) recorded in situ for various films of PEOpy-49 on oxidized silicon during crystallization at 45 °C.

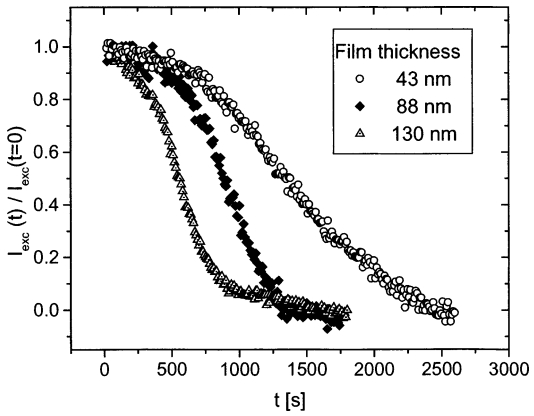

Figure 11. Normalized[80] steady-state fluorescence emission intensity at 480 nm measured for different films of PEOpy-49 on oxidized silicon. The data were acquired in situ at $T_c = 50$ °C.

the polymer chain orientation, the lamellar crystal orientation, and the probability of finding pyrene end groups in close proximity. The spectroscopic data also show a pronounced decrease in crystallization rates and degree of crystallinity for films thinner than 100 nm.

The analysis of the half-crystallization times indicated that the confinement of PEO in ultrathin films slows down the growth of lamellar crystals considerably when film thicknesses become less than ca. 100−200 nm. Interestingly, the $\tau_{1/2}$ measured in the FT-IR spectra was significantly longer than the half-crystallization times deduced from the fluorescence spectroscopy experiments (Figure 12). This observation can be understood since the changes in the absorbance of the band at 1344 cm^{-1} in the FT-IR spectra correspond to the increasing fraction of conformationally ordered PEO helices, while the variations in excimer emission intensity provide information only about the proximity of the chain ends. While the distribution of chain-end distances changes as the material crystallizes, these changes seem to occur much more rapidly than the increase in conformational order or crystallinity of the PEO molecules. Thus, while the chain ends have a near-constant mean distance, the chain segments continue to crystallize. This observation may be related to increasing perfection of the lamellar crystals or secondary crystallization of PEO confined to the interstitial spaces between the initially grown lamellae.

Since it is not a priori clear how to convert the measured fluorescence emission intensity changes during crystallization to the fraction of crystallized material, a more elaborate treatment of the crystallization

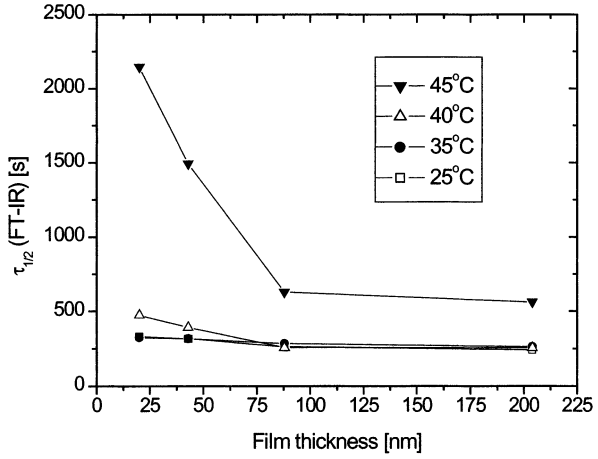

a

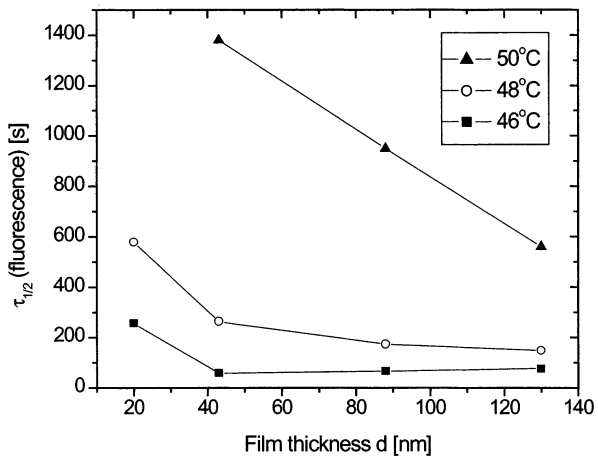

b

Figure 12. Plot of half-crystallization times for crystallization of different films of PEO-py-49 on oxidized silicon at various temperatures estimated from (a) the integrated intensity at 1344 cm^{-1} (FT-IR) and (b) the excimer fluorescence intensity.

kinetics was attempted for the FT-IR data only. If we assume that the absorbance observed at 1344 cm^{-1} is exclusively due to the absorption of infrared radiation by the crystalline phase,[68] the changes in absorbance are to a first approximation proportional to the changes in degree of crystallinity. The data have been fitted to a linearized form of the following general Avrami equation[22,49,76]

$$1 - (V_c/V_\infty) = \exp(-Kt^n) \qquad (1)$$

where V_c and V_∞ denote the volume of crystallized material at time t and the volume of crystallized material at time ∞, respectively, K is a rate constant, t is the time, and n is the Avrami exponent.

We have selected only the initial stages of crystallization for the analysis. The linearized Avrami plots for different film thicknesses could be fitted with satisfactory results (Figure 13). The data for the thinnest film, however, are noisy due to the limited number of scans averaged in this kinetic experiment. While the slopes and, hence, the Avrami exponent are very similar for all films, the intercepts decrease with decreasing film thickness, especially when the films are thinner than

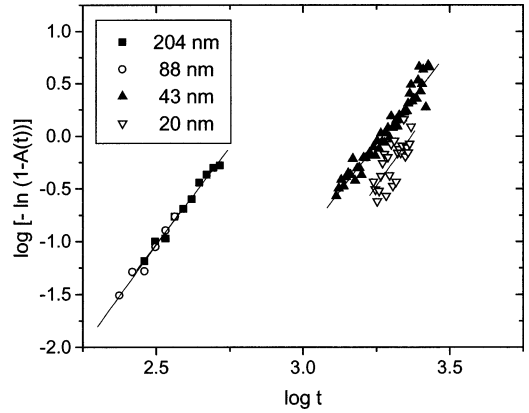

Figure 13. Linearized Avrami plot and linear fits for various PEOpy-49 films crystallized isothermally on oxidized silicon at 45 °C.

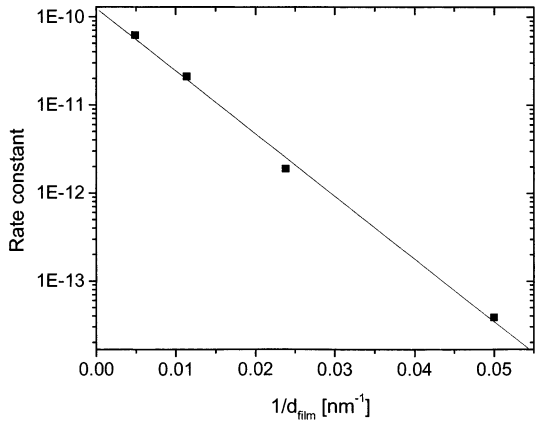

Figure 14. Empirical fit to the rate constants obtained from the Avrami analysis for data obtained at 45 °C.

Table 2. Avrami Exponent *n* and Rate Constant Determined from in Situ FT-IR Measurements of PEOpy-49 Crystallized in Thin Films at 45 °C

film thickness [nm]	Avrami exponent	rate constant K
204	3.7	6.2×10^{-11}
88	3.9	2.1×10^{-11}
42	3.6	1.9×10^{-12}
20	4.0	3.9×10^{-14}

88 nm. The data for the 204 and 88 nm are almost identical, which suggests that the crystallization kinetics, as sampled by FT-IR, are only affected markedly for very thin films.

The dimensionality of growth for the crystallization is not significantly affected by the confinement into ultrathin films, as shown in Table 2. This observation is consistent with the AFM observation of the same lamellar morphology of the crystallized material. For PEOpy-49 crystallized at 45 °C, an Avrami exponent n between 3 and 4 is found, which would correspond to either 2-D ($n = 3$) or 3-D ($n = 4$) crystallization under thermal conditions.[76,77] The rate constant, however, is a strong function of film thickness and can be empirically described by an exponential relationship ($G_{norm} \propto \exp[-(1/d)]$ (Figure 14). Interestingly, a very similar relationship is found based on in situ AFM data for crystallization of *individual* lamellae from self-seeded melts.[53,55c] Moreover, for the crystallization of PEO in block copolymers with a lamellar morphology (lamellar thickness of PEO block $\sim$ 8.8 nm), it has been reported that the Avrami rate constant was decreased considerably compared to crystallization in the bulk.[78]

The crystallization rates were retarded as shown above for thickness of ca. 100 nm and below. Similarly, by hot stage AFM the growth rates of PEO on oxidized silicon were found to be retarded for film thicknesses below ca. 200 nm.[55c,56] These thicknesses exceed the radii of gyration (R_g) by many times. For the PEO materials studied, the R_g are less than ca. 11 nm, which means that the interface is screened for most thicknesses studied.[79] However, the glass transition temperatures[14−21] and mobilities[37−41] of various polymers in thin and ultrathin films were found to be affected over similarly large distances.

For the crystallization of isotactic polystyrene (iPS) in ultrathin films, Sawamura et al. observed that the normalized growth rate is a function of (1 − constant/d); they interpreted this result as implying a reduction of the tube diameter for reptation of the polymer molecules through the melt.[24a] The film thickness dependence of the lamellar growth rate found in our studies[53,55] is much stronger than reported for iPS (Figure 14). As shown in the companion paper,[55c] the growth rates of PEO can be successfully described by the Hoffman−Lauritzen theory, and the depression of the growth rates with decreasing film thickness can be taken into account by an adjusted transport term of the Hoffman−Lauritzen equation for the growth rate. This adjustment is a constant offset and corresponds to an increase of the glass transition temperature as a function of decreasing film thickness. An increase in T_g is physically reasonable[36] and would result in a slower diffusion of polymer molecules to the growth front of the growing lamellae. We cannot compare the iPS work cited and our data directly, but it is likely that the expected changes in T_g may have a different distance dependence, leading to a different film thickness dependence of the growth rate depression.

For ultrathin films of poly(di-*n*-hexylsilane), the Avrami analysis yielded a nearly thickness- and temperature-independent rate constant, while the dimensionality of the growth (Avrami exponent n) was very sensitive to both film thickness and crystallization temperature.[2,22] Interestingly, for films thinner than 15 nm there was no detectable crystallinity. A direct comparison of our data on PEO with the poly(di-*n*-hexylsilane) ultrathin films is difficult since the preferred chain orientation is completely different. While PEO crystallizes with the polymer helices oriented along the surface-normal direction (Figures 3−5), poly(di-*n*-hexylsilane) crystallizes with the chains oriented parallel to the plane of the film,[2,23] similar to many polyolefins.[53] Zhu et al. reported that the orientation of the primary nuclei does not determine the direction of growth of PEO in the confinement of lamellar block copolymers, but rather that the initial stages of crystal growth determine this direction.[11] If this observation can be generalized and chain orientation is driven by interfacial interactions,[45] the two limiting cases of preferential chain orientation can be expected to lead to a distinct crystallization behavior. For chain orientation along the surface-normal direction, crystallization should remain possible for all film thicknesses d, even if the lamellar thickness L exceeds d. Consequently, very thin crystallized films may rupture due to lack of material when $L > d$ but still crystallize in the covered areas. In fact, we have observed by hot stage AFM that ultrathin PEO films may crystallize with $L > d$ and that films below 15 nm tend to break up and crystallize with a dendritic habit (compare Figure S1 of Supporting Information).[55c] In addition, Reiter and Sommer showed that PEO monolayers can be crystallized on silicon substrates.[44] On the other hand, for polymers that favor a chain orientation in the plane of the film, the growth may be inhibited when the film thickness decreases below a certain threshold value that may be related to the critical size of the nucleus. This behavior has been experimentally verified for poly(di-*n*-hexylsilane).[2,22,23]

On the basis of the data discussed here, it becomes clear that the morphology and structure, as well as the average crystallization kinetics of PEO and pyrene end-labeled PEO, are affected significantly by the confinement of the material in ultrathin films. The altered properties may be attributed to the presence of two different interfaces. The oxidized silicon substrate presents an interactive surface, while the atmosphere (air) may be interpreted as noninteractive surface. Interactions of the polymer molecules with the interfaces should lead to an altered glass transition temperature.[36] The glass transition temperature is coupled to the chain mobility and hence diffusion of polymer in the melt and therefore affects the crystallization kinetics considerably. In fact, a similar observation has been reported for blends of PEO with PMMA.[68] Since we observe a clear decrease in growth rate for crystallization in ultrathin films as compared to thick films, this suggests that the substrate−polymer interface dominates the physics of the ultrathin polymer films.

Summary

Isothermally crystallized thin and ultrathin films of poly(ethylene oxides) on oxidized silicon substrates were characterized by a combination of in situ hot stage AFM, multimode FT-IR, and fluorescence spectroscopy. As shown by AFM and FT-IR, lamellar crystals grow preferentially in flat-on orientation in films thinner than ca. 300 nm; i.e., the helices of PEO are oriented along the surface-normal direction. By contrast, the orientation of lamellar crystals is preferentially edge-on in films thicker than ca. 1 μm. In addition, FT-IR reveals that the preferential orientation depends strongly on film thickness, but not on crystallization temperature for low undercoolings, and that the degree of crystallinity decreases with decreasing film thickness. The excimer/monomer ratios observed in steady-state fluorescence emission spectra for pyrene end-labeled polymers show a marked dependence on crystallization temperature and film thickness. These observations can be interpreted in accordance with a crystallization temperature-dependent distribution of excimer site energies and a dilution of pyrene in the increased fraction of amorphous phase of PEO in very thin films, respectively. The presence of an interactive substrate surface, i.e., SiO_2, slows down the crystallization process as measured by FT-IR and fluorescence spectroscopy in situ. The FT-IR spectroscopic results agree well with in situ hot stage AFM data reported in a separate paper.

Acknowledgment. The authors thank Larry E. Bailey and Qingrong Huang for their contributions in building the hot stages and Clemens Padberg (University of Twente) for carrying out the GPC analysis of the PEOpy materials. H.S. gratefully acknowledges financial support by the Deutsche Akademischer Austauschdienst (DAAD) in the framework of the

"Hochschulsonderprogramm III" and the NSF MRSEC Center on Polymer Interfaces and Macromolecular Assemblies (CPIMA) under DMR 9808677.

Supporting Information Available: TM-AFM height image of PEO-49Py (film thickness 7 nm), transmission mode FT-IR spectra of PEO films on oxidized silicon (all materials), logarithmic plot of excimer/monomer emission intensity vs film thickness for PEOpy-49 on oxidized silicon, and normalized steady-state fluorescence emission spectra of PEOpy-49 on oxidized silicon recorded at different temperatures. This material is available free of charge via the Internet at http://pubs.acs.org.

References and Notes

(1) *Physics of Polymer Surfaces and Interfaces*; Sanchez, I. C., Ed.; Butterworth-Heinemann: Boston, 1992.
(2) Frank, C. W.; Rao, V.; Despotopoulou, M. M.; Pease, R. F. W.; Hinsberg, W. D.; Miller, R. D.; Rabolt, J. F. *Science* **1996**, *273*, 912 and references cited therein.
(3) Hietpas, G. D.; Sands, J. M.; Allara, D. L. *J. Phys. Chem. B* **1998**, *102*, 10556 and references cited therein.
(4) See e.g.: Pike, C.; Bell, S.; Lyons, C.; Plat, M.; Levinson, H.; Okoroanyanwu, U. *J. Vac. Sci. Technol. B* **2000**, *18*, 3360.
(5) Johnson, K. E.; Mate, C. M.; Merz, J. A.; White, R. L.; Wu, A. W. *IBM J. Res. Develop.* **1996**, *40*, 511 and references cited therein.
(6) Yang, X. G.; Shi, J. X.; Johnson, S.; Swanson, B. *Langmuir* **1998**, *14*, 1505.
(7) Walheim, S.; Schaffer, E.; Mlynek, J.; Steiner, U. *Science* **1999**, *283*, 520.
(8) Decher, G. *Science* **1997**, *277*, 1232.
(9) Donath, E.; Sukhorukov, G. B.; Caruso, F.; Davis, S. A.; Möhwald, H. *Angew. Chem., Int. Ed.* **1998**, *37*, 2202.
(10) Weimann, P. A.; Hajduk, D. A.; Chu, C.; Chaffin, K. A.; Brodil, J. C.; Bates, F. S. *J. Polym. Sci., Part B: Polym. Phys.* **1999**, *37*, 2053.
(11) Zhu, L.; Cheng, S. Z. D.; Calhoun, B. H.; Ge, Q.; Quirk, R. P.; Thomas, E. L.; Hsiao, B. S.; Yeh, F.; Lotz, B. *Polymer* **2001**, *42*, 5829 and references cited therein.
(12) Hong, S.; MacKnight, W. J.; Russell, T. P.; Gido, S. P. *Macromolecules* **2001**, *34*, 2876.
(13) Anastasiadis, S. H.; Karatasos, K.; Vlachos, G.; Manias, E.; Giannelis, E. P. *Phys. Rev. Lett.* **2000**, *84*, 915.
(14) Keddie, J. L.; Jones, R. A. L.; Cory, R. A. *Europhys. Lett.* **1994**, *27*, 59.
(15) Keddie, J. L.; Jones, R. A. L.; Cory, R. A. *Faraday Discuss.* **1994**, *98*, 219.
(16) Forrest, J. A.; Mattson, J. *Phys. Rev. E* **2000**, *61*, R53 and references cited therein.
(17) Prucker, O.; Christian, S.; Bock, H.; Rühe, J.; Frank, C. W.; Knoll, W. *Macromol. Chem. Phys.* **1998**, *199*, 1435.
(18) DeMaggio, G. B.; Frieze, W. E.; Gidley, D. W.; Zhu, M.; Hristov, H. A.; Yee, A. F. *Phys. Rev. Lett.* **1997**, *78*, 1524.
(19) Jones, R. A. L. *Curr. Opin. Colloid Interface Sci.* **1999**, *4*, 153.
(20) Kim, J. H.; Jang, J.; Zin, W. C. *Langmuir* **2001**, *17*, 2703.
(21) van Zanten, J. H.; Wallace, W. E.; Wu, W. L. *Phys. Rev. E* **1996**, *53*, R2053.
(22) Despotopoulou, M. M.; Frank, C. W.; Miller, R. D.; Rabolt, J. F. *Macromolecules* **1996**, *29*, 5797.
(23) Despotopoulou, M. M.; Frank, C. W.; Miller, R. D.; Rabolt, J. D. *Macromolecules* **1995**, *28*, 6687. (b) Despotopoulou, M. M.; Miller, R. D.; Rabolt, J. D.; Frank, C. W. *J. Polym. Sci., Part B: Polym. Phys.* **1996**, *34*, 2335.
(24) Sawamura, S.; Miyaji, H.; Izumi, K.; Sutton, S. J.; Miyamoto, Y. *J. Phys. Soc. Jpn.* **1998**, *67*, 3338. (b) Sutton, S. J.; Izumi, K.; Miyaji, H.; Miyamoto, Y.; Miyatashi, S. *J. Mater. Sci.* **1997**, *32*, 5621.
(25) Krausch, G.; Dai, C.-A.; Kramer, E. J.; Marko, J. F.; Bates, F. S. *Macromolecules* **1993**, *26*, 5566.
(26) Meuse, C. W.; Yang, X.; Yang, D.; Hsu, S. L. *Macromolecules* **1992**, *25*, 925. (b) Tao, H.-J.; Meuse, C. W.; Yang, X.; MacKnight, W. J.; Hsu, S. L. *Macromolecules* **1994**, *27*, 7146.
(27) Fasolka, M. J.; Banerjee, P.; Mayes, A. M.; Pickett, G.; Balazs, A. C. *Macromolecules* **2000**, *33*, 5701.
(28) Pfromm, P. H.; Koros, W. J. *Polymer* **1995**, *36*, 2379.
(29) Liang, T.; Makita, Y.; Kimura, S. *Polymer* **2001**, *42*, 4867.
(30) Beck Tan, N. C.; Wu, W. L.; Wallace, W. E.; Davis, G. T. *J. Polym. Sci., Part B: Polym. Phys.* **1998**, *36*, 155.
(31) Reiter, G. *Europhys. Lett.* **1993**, *23*, 579.
(32) Kraus, J.; Müller-Buschbaum, P.; Kuhlmann, T.; Schubert, D. W.; Stamm, M. *Europhys. Lett.* **2000**, *49*, 210.
(33) Ten Brinke, G.; Ausserre, D.; Hadziioannou, G. *J. Chem. Phys.* **1988**, *89*, 4374. (b) Kumar, S. K.; Vacatello, M.; Yoon, D. Y. *J. Chem. Phys.* **1988**, *89*, 5207. (c) Bitsanis, I.; Hadziioannou, G. *J. Chem. Phys.* **1990**, *92*, 3827.
(34) Jones, R. A. L.; Kumar, S. K.; Ho, D. L.; Briber, R. M.; Russell, T. P. *Nature (London)* **1999**, *400*, 146.
(35) For a review on T_g depressions in ultrathin films, see: Tseng, K. C.; Turro, N. J.; Durning, C. J. *Phys. Rev. E* **2000**, *61*, 1800.
(36) Fryer, D. S.; Nealey, P. F.; de Pablo, J. J. *Macromolecules* **2000**, *33*, 6439. (b) Torres, J. A.; Nealey, P. F.; dePablo, J. J. *Phys. Rev. Lett.* **2000**, *85*, 3221.
(37) Frank, B.; Gast, A. P.; Russell, T. P.; Brown, H. R.; Hawker, C. *Macromolecules* **1996**, *29*, 6531.
(38) Zheng, X.; Rafailovich, M. H.; Sokolov, J.; Strzhemechny, Y.; Schwarz, S. A.; Sauer, B. B.; Rubinstein, M. *Phys. Rev. Lett.* **1997**, *79*, 241.
(39) Zheng, X.; Sauer, B. B.; van Alsten, J. G.; Schwarz, S. A.; Rafailovich, M. H.; Sokolov, J.; Rubinstein, M. *Phys. Rev. Lett.* **1995**, *74*, 407.
(40) Russell, T. P.; Kumar, S. K. *Nature (London)* **1997**, *386*, 771.
(41) Lin, E. K.; Kolb, R.; Satija, S. K.; Wu, W.-L. *Macromolecules* **1999**, *32*, 3753.
(42) Tseng, K. C.; Turro, N. J.; Durning, C. J. *Polymer* **2000**, *41*, 4751.
(43) Hall, D. B.; Torkelson, J. M. *Macromolecules* **1998**, *31*, 8817.
(44) Reiter, G.; Sommer, J.-U. *Phys. Rev. Lett.* **1998**, *80*, 3771. (b) Reiter, G.; Sommer, J.-U. *J. Chem. Phys.* **2000**, *112*, 4376.
(45) Bartczak, Z.; Argon, A. S.; Cohen, R. E.; Kowalewski, T. *Polymer* **1999**, *40*, 2367.
(46) Srinivas, S.; Babu, J. R.; Riffle, J. S.; Wilkes, G. L. *J. Macromol. Sci., Phys.* **1997**, *B36*, 455.
(47) The growth rate G is proportional to $\exp(-U^*/[R(T_c - [T_g - 30\ \mathrm{K}])]$, where U^* denotes the activation energy for reptation motion across the melt−crystal interface, R is the gas constant, T_c is the crystallization temperature, and T_g is the glass transition temperature. For details, see: Hoffman, J. D.; Miller, R. L. *Macromolecules* **1989**, *22*, 3502 and cited references.
(48) Vaia, R. A.; Sauer, B. B.; Tse, O. K.; Giannelis, E. P. *J. Polym. Sci., Part B: Polym. Phys.* **1997**, *35*, 59.
(49) Avrami, M. *J. Chem. Phys.* **1939**, *7*, 1103.
(50) Hoffman, C. L.; Rabolt, J. F. *Macromolecules* **1996**, *29*, 2543.
(51) Muratoglu, O. K.; Argon, A. S.; Cohen, R. E. *Polymer* **1995**, *36*, 2143.
(52) Hietpas, G. D.; Allara, D. L. *J. Polym. Sci., Part B: Polym. Phys.* **1998**, *36*, 1247.
(53) Schönherr, H.; Waymouth, R. M.; Hawker, C. J.; Frank, C. W. *ACS Polym. Mater.: Sci. Eng.* **2001**, *84*, 453.
(54) Schönherr, H.; Waymouth, R. M.; Frank, C. W., manuscript in preparation.
(55) This paper. (b) Schönherr, H.; Bailey, L. E.; Frank, C. W. *Langmuir* **2002**, *18*, 490. (c) Schönherr, H.; Frank, C. W. *Macromolecules* **2003**, *36*, 1199.
(56) In the course of writing this manuscript a similar study has been published by Dalnoki-Veress et al., which describes the reduction of crystallization rates for PEO thin films on silicon and gold substrates as studied by quartz crystal microbalance and video optical microscopy (Dalnoki-Veress, N.; Forrest, J. A.; Massa, M. V.; Pratt, A.; Williams, A. *J. Polym. Sci., Part B: Polym. Phys.* **2001**, *39*, 2615). The complementary results reported by these authors are in good agreement with our data.
(57) Kovacs, A. J.; Gonthier, A. *Kolloid Z. Z. Polym.* **1972**, *250*, 530. (b) Marentette, J. M.; Brown, G. R. *Polymer* **1998**, *39*, 1405 and references cited therein.
(58) Takahashi, Y.; Tadokoro, H. *Macromolecules* **1973**, *6*, 672.
(59) Takahashi, Y.; Sumita, I.; Tadokoro, H. *J. Polym. Sci., Part B: Polym. Phys.* **1973**, *11*, 2113.
(60) Pearce, R.; Vancso, G. J. *Macromolecules* **1997**, *30*, 5843. (b) Pearce, R.; Vancso, G. J. *Polymer* **1998**, *39*, 1237. (c) Schultz, J. M.; Miles, M. J. *J. Polym. Sci., Part B: Polym. Phys.* **1998**, *36*, 2311.
(61) The PEOpy materials were available from previous studies. GPC was measured relative to PS in chloroform at the Department of Materials Science and Technology of Polymers, University of Twente, Enschede, The Netherlands.
(62) Gullerud, S. Ph.D. Thesis, Stanford University, 1999.
(63) Because of heat generated by the AFM, this corresponds to a true sample temperature of ca. 34 °C.
(64) In thick films there is a coexistence of edge-on and flat-on lamellae.

(65) Bassett, D. C. *Principles of Polymer Morphology*; Cambridge University Press: Cambridge, 1981.
(66) Yoshihara, T.; Tadokoro, H.; Murahashi, S. *J. Chem. Phys.* **1964**, *41*, 2902.
(67) Allara, D. L. In *Characterization of Organic Thin Films*; Ulman, A., Ed.; Butterworth-Heinemann: Boston, 1994; Chapter 4.
(68) Li, X.; Hsu, S. L. *J. Polym. Sci., Polym. Phys.* **1984**, *22*, 1331.
(69) As shown in the Supporting Information (Figure S2), the transmission FT-IR spectra of PEO-100, PEOpy-49, PEOpy-29, and PEOpy-11 after isothermal crystallization at 44 °C were very similar.
(70) For samples that are quenched to room temperature or below, the absorbance ratio does indeed indicate a more random orientation of the rapidly crystallized PEO helices.
(71) Jing, S.; Qiao, C.; Tian, S.; Ji, X.; An, L.; Jiang, B. *Polymer* **2001**, *42*, 5755.
(72) Lakowicz, J. R. *Principles of Fluorescence Spectroscopy*; Kluwer Academic/Plenum: New York, 1999.
(73) Chen, S. H.; Frank, C. W. *Langmuir* **1991**, *7*, 1719 and references cited therein.
(74) PEOpy-29 showed qualitatively similar behavior, while the strong excimer fluorescence dominated the spectra for PEOpy-11.
(75) Frank, C. W. *J. Chem. Phys.* **1974**, *61*, 2015.
(76) Gedde, U. *Polymer Physics*, 1st ed.; Kluwer Academic Publishers: Dordrecht, 1995.
(77) Because of the limited time resolution of the experiment and the low probability to nucleate crystals at higher temperatures in unseeded melts, it is difficult to study a broad range of crystallization temperatures by FT-IR.
(78) For these block copolymers the dimensionality of the growth was also a function of crystallization temperature; see ref 11.
(79) R_g values were calculated from the weight-average molecular weight M_w according to eq 2: $R_g = 0.0304\sqrt{M_w}$ (in nm). This relation is based on SANS results for PEO with $M_w = 27$ kg/mol that yielded $R_g = 5$ nm (Annis, B. K.; Kim, M.-H.; Wignall, G. D.; Borodin, O.; Smith, G. D. *Macromolecules* **2000**, *33*, 7544). For PEO-100, PEOpy-49, PEOpy-29, and PEOpy-11 we obtained R_g values of 10.8, 7.6, 5.8, and 3.5 nm, respectively.
(80) Because of instrumental limitations we can follow the fluorescence intensity at a single emission wavelength only. Thus, it was impossible to acquire simultaneously the monomer and excimer emission intensities during crystallization. The data shown in Figure 11 represent the changes in *excimer* emission intensity during the crystallization of the PEO film. During crystallization the monomer emission intensity also decreases or increases depending on film thickness. Any of these changes in emission intensity must be related to the crystallization process since we crystallize under isothermal conditions. Hence, these changes may serve as an independent means to characterize the effect of confinement on the crystallization kinetics.

MA020685I